Manipulation of spin-wave attenuation and polarization in antiferromagnets

Zhi-ming Yan ⬡, Zhi-xiong Li, Xi-guang Wang, Zi-yan Luo, Qing-lin Xia, Yao-zhuang Nie, and Guang-hua Guo ⬡*

School of Physics and Electronics, Central South University, Changsha 410083, China

The coexistence of a left-handed polarized spin wave (LPSW) and a right-handed polarized spin wave (RPSW) in antiferromagnets provides a scheme for designing novel magnonic devices. To do so, it is necessary to manipulate the attenuation and the polarization of the LPSW and RPSW separately. We address this issue by studying theoretically the effect of spin-transfer torques (STTs) and an external magnetic field on spin waves (SWs) propagating in antiferromagnets. We find that Slonczewski-type STT can increase the attenuation length of one of the SW modes and decrease that of the other, while Zhang-Li type STT enhances (or weakens) the attenuation of both the LPSW and the RPSW simultaneously. Using the combined effect of the two kinds of STTs or the STT and an external magnetic field, we demonstrate control of the LPSW and RPSW attenuations separately, thus we can manipulate the SW polarization. We further suggest a magnon spin filter that can filter out one of the SW modes and preserve the other, which generates a pure magnonic spin current in antiferromagnets.

INTRODUCTION

Antiferromagnetic (AFM) spintronics has a great deal of potential for application in high packing density and high-speed magnetic random access memories (MRAMs), neuromorphic computing, and ultrafast information technology [1–7], stemming from a zero stray field and THz spin dynamics. A number of breakthroughs have been made in the field of AFM spintronics. Electric-current-induced magnetization switching has been achieved experimentally in AFM CuMnAs [8] and Mn_2Au [9] as well as in AFM/heavy-metal heterostructures [10,11]. Spin transfer torque (STT) has been used to control the ground states in three sublattice noncollinear antiferromagnets and to reach deterministic switching between states [12]. In addition, electrical readout has been realized in antiferromagnetism by means of anisotropic magnetoresistance (AMR), spin Hall MR, and the anomalous Hall effect [13–16].

Important progress has also been made in the study of AFM magnonics. The spin Seebeck effect was found in $Cr_2O_3(MnF_2)$/Pt heterostructures [17–19]. Magnonic spin current was generated in Cr_2O_3 and MnF_2 by the spin pumping effect [20–22]. The injection of spin currents into antiferromagnets was achieved through ferromagnetic (FM)/AFM or heavy-metal (topological insulator)/AFM interfaces [23–25], and three magnon transmission states were found in an antiferromagnetically coupled trilayer magnonic spin valve [26]. Moreover, the manipulation of spin-wave (SW) polarization in an antiferromagnet was demonstrated theoretically via the domain-wall [27] or curvilinear effects of AFM wires [28], and the SW propagating characteristics in a ferrimagnet near the compensation point were studied

[29]. In antiferromagnetism, the right-handed polarized SW (RPSW) and the left-handed polarized SW (LPSW) coexist due to two antiparallel magnetic sublattices. Therefore, in addition to the amplitude and phase, the SW polarization can be exploited to code information in an antiferromagnet [30], and the spin transistor is more easily realized based on the magnonic spin in the antiferromagnet [31]. However, due to the degeneracy of the LPSW and the RPSW, the SW transport in the antiferromagnet generally does not produce a magnonic spin current. The generation of the magnonic spin current in the antiferromagnet needs to break the symmetry of the two magnetic sublattices. To design AFM magnonic devices, one must know how to manipulate the LPSW and RPSW separately and generate the magnonic spin current effectively.

In antiferromagnetism, the splitting of the LPSW and RPSW dispersion relations can be realized by various methods. The most direct way is to apply an external magnetic field; however, usually a large field is required to obtain a moderate splitting [32]. Liang *et al.* [33] found that the LPSW and RPSW dispersion relations in an AFM domain wall will split into four separate bands with specific polarities when the interfacial Dzyaloshinskii-Moriya interaction (DMI) is taken into account. In addition, it has been demonstrated that the magnon spectrum can be split by combining the strain or DMI with an adiabatic STT [34]. Furthermore, Kim *et al.* [35] have shown that the splitting of the circularly polarized magnon spectrum occurs when magnons pass through a rotating domain wall.

In this work, using analytical calculations and micromagnetic simulations, we study the propagating characteristics of an LPSW and an RPSW in an antiferromagnet and the tuning effect of Slonczewski-type STT [36–38], Zhang-Li type STT [39,40], as well as the external magnetic field. Our studies provide a way to manipulate the attenuation of the LPSW and RPSW separately so that we can control the polarization of SWs. We further suggest a magnon spin filter that can filter out

---

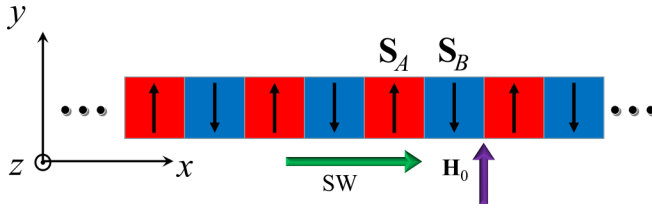*Author to whom correspondence should be addressed: guogh@mail.csu.edu.cn

134432-1

FIG. 1. Schematics of the one-dimensional antiferromagnetic chain. The magnetic moments are along the positive or negative y-axis. The spin waves propagate along the x-axis.

one of the SW modes and preserve the other so as to generate a pure magnonic spin current in an antiferromagnet.

II. MODEL AND APPROACH

We consider a one-dimensional AFM chain as shown in Fig. 1. $\mathbf{S}_A$ and $\mathbf{S}_B$ are the spin moments at A and B sublattice sites, respectively, and they are directed oppositely along the y-axis. Here we suppose $S = |\mathbf{S}_A| = |\mathbf{S}_B|$. The Hamiltonian of the system includes exchange, uniaxial anisotropy, and Zeeman energies, which can be expressed as [41,42]

$$E = 2J \sum_{\langle A,B \rangle}^{N,N} \mathbf{S}_A \cdot \mathbf{S}_B - K \sum_i^N [(S_{A,iy})^2 + (S_{B,iy})^2]$$
$$- \gamma \hbar \sum_i^N (\mathbf{S}_{A,i} + \mathbf{S}_{B,i}) \cdot \mathbf{H}_0, \tag{1}$$

where N is the number of the primitive cell in the system, and i denotes the ith primitive cell. J is the exchange constant between A and B sublattices, $\langle A, B \rangle$ denotes a sum over all nearest-neighbor lattice sites, K is the uniaxial anisotropy constant with the easy magnetization direction along the y-axis, γ is the gyromagnetic ratio, and $\hbar$ is the reduced Planck constant. $\mathbf{H}_0 = H_0 \hat{\mathbf{y}}$ represents the external magnetic field.

The effective magnetic fields acting on the sublattices are given by $-\frac{1}{\gamma \hbar} \frac{\partial E}{\partial \mathbf{S}_i}$:

$$\mathbf{H}_{A,i} = \mathbf{H}_0 + H_a(\mathbf{m}_{A,i} \cdot \hat{\mathbf{y}})\hat{\mathbf{y}} - \frac{H_e(\mathbf{m}_{B,i-1} + \mathbf{m}_{B,i})}{2},$$
$$\mathbf{H}_{B,i} = \mathbf{H}_0 + H_a(\mathbf{m}_{B,i} \cdot \hat{\mathbf{y}})\hat{\mathbf{y}} - \frac{H_e(\mathbf{m}_{A,i} + \mathbf{m}_{A,i+1})}{2}, \tag{2}$$

where $\mathbf{m}_{A,i} = \mathbf{S}_{A,i}/S$ and $\mathbf{m}_{B,i} = \mathbf{S}_{B,i}/S$ denote the unit vectors along the local spin moments. The effective exchange field H_e and anisotropy field H_a are defined by $H_e = 4SJ/g\hbar$ and $H_a = 2SK/g\hbar$, respectively.

The magnetization dynamics of the antiferromagnet is governed by the Landau-Lifshitz-Gilbert (LLG) equation including the STT [43],

$$\frac{\partial \mathbf{m}_{A,i}}{\partial t} = -\gamma \mathbf{m}_{A,i} \times \mathbf{H}_{A,i} + \alpha \mathbf{m}_{A,i} \times \frac{\partial \mathbf{m}_{A,i}}{\partial t} + \boldsymbol{\tau}_{A,i},$$
$$\frac{\partial \mathbf{m}_{B,i}}{\partial t} = -\gamma \mathbf{m}_{B,i} \times \mathbf{H}_{B,i} + \alpha \mathbf{m}_{B,i} \times \frac{\partial \mathbf{m}_{B,i}}{\partial t} + \boldsymbol{\tau}_{B,i}. \tag{3}$$

α is the Gilbert damping constant, and $\boldsymbol{\tau}_{A,i}$ ($\boldsymbol{\tau}_{B,i}$) represents the STT acting on the $\mathbf{m}_{A,i}$ ($\mathbf{m}_{B,i}$). Here we consider two types of STT. One is Slonczewski-type STT, which has the form

[36–38]

$$\boldsymbol{\tau}_{A,i} = c(\mathbf{m}_{A,i} \times \mu \times \mathbf{m}_{A,i}),$$
$$\boldsymbol{\tau}_{B,i} = c(\mathbf{m}_{B,i} \times \mu \times \mathbf{m}_{B,i}), \tag{4}$$

where c is the strength of the STT, which is proportional to the electric current density, and μ is the spin polarization vector; here we set $\mu = (0, 1, 0)$. The Slonczewski-type STT can be generated in magnetic multilayers [37], and the strength can be expressed as $c = g\mu_B P J_c 1/2eM_s d$. Here g is the Landé factor, μ_B is the Bohr magneton, $J_c 1$ and P denote the current density and spin polarization, respectively, e is the electron charge, M_s is the saturation magnetization, and d is the thickness of the AFM layer. The Slonczewski-type STT can also be induced in an AFM/heavy-metal heterostructure [10,11].

Another kind of STT is the Zhang-Li type, which is induced by the electric current flowing in AFMs, and it can be expressed as [39,40]

$$\boldsymbol{\tau}_{A,i} = (\mathbf{u}_A \cdot \nabla)\mathbf{m}_{A,i} - \beta \mathbf{m}_{A,i} \times (\mathbf{u}_A \cdot \nabla)\mathbf{m}_{A,i},$$
$$\boldsymbol{\tau}_{B,i} = (\mathbf{u}_B \cdot \nabla)\mathbf{m}_{B,i} - \beta \mathbf{m}_{B,i} \times (\mathbf{u}_B \cdot \nabla)\mathbf{m}_{B,i}, \tag{5}$$

where $\mathbf{u}_A/B$ is the magnitude of adiabatic STT acting on the $\mathbf{m}_A/B$, and it can be written as $\mathbf{u}_A/B = (g\mu_B P_A/BJ_c 2/2eM_s) \hat{\mathbf{x}}$. Here $J_c 2$ is the electric current density, P_A/B is the spin polarization of each sublattice, and β is the ratio of the nonadiabatic to adiabatic STT. In our model, the two sublattices are equivalent, thus $P_A = P_B$, $\mathbf{u}_A = \mathbf{u}_B = u\hat{\mathbf{x}}$.

In general, the magnetic field generates a Lorentz force acting on the itinerant electrons, which will influence the motion of electrons. Moreover, the magnetic field acts on the electron spin, giving rise to the Hanle effect. In our micromagnetic study based on the LLG equation, neither effect is considered (as what is done in the literature [43,44]).

We consider the spin waves propagating in the x-axis, and we set $\mathbf{m}_{A,i}$ ($\mathbf{m}_{B,i}$) as [45,46]

$$\mathbf{m}_{A,i} = \left(m_{Ax_0} e^{i(kx_i - \omega t) - x_i/\Lambda}, 1, m_{Az_0} e^{i(kx_i - \omega t) - x_i/\Lambda} \right),$$
$$\mathbf{m}_{B,i} = \left(m_{Bx_0} e^{i(kx_i - \omega t) - \frac{x_i}{\Lambda}}, -1, m_{Bz_0} e^{i(kx_i - \omega t) - \frac{x_i}{\Lambda}} \right), \tag{6}$$

where Λ is the SW attenuation length, and ω and k are the SW frequency and wave vector, respectively. Substituting Eq. (6) into Eq. (3), we obtain the dispersion relations and attenuation lengths of SWs (details are provided in the Supplemental Material [47]).

For numerical calculations, the parameters corresponding to the material KMnF$_3$ are used [48]: $J = 5.25 \times 10^{-22}$ J, $K = 2.29 \times 10^{-24}$ J, $M_s = 3.76 \times 10^5$ A/m, and lattice constant $a = 0.5$ nm. To verify the theoretical predictions, we also perform full micromagnetic simulations using MuMax3 [49]. The AFM structure we study is an AFM nanowire with grid size $10\,000 \times 1 \times 1$ and cell size 0.5 nm $\times$ 0.5 nm $\times$ 0.5 nm. The Gilbert damping constant is $\alpha = 0.001$ to ensure a proper propagation distance of SWs. An exponentially increased damping α near the edges is adopted as an absorbing boundary condition to prevent the reflection of SWs. Additional details of the micromagnetic simulations are provided in the Supplemental Material [47].
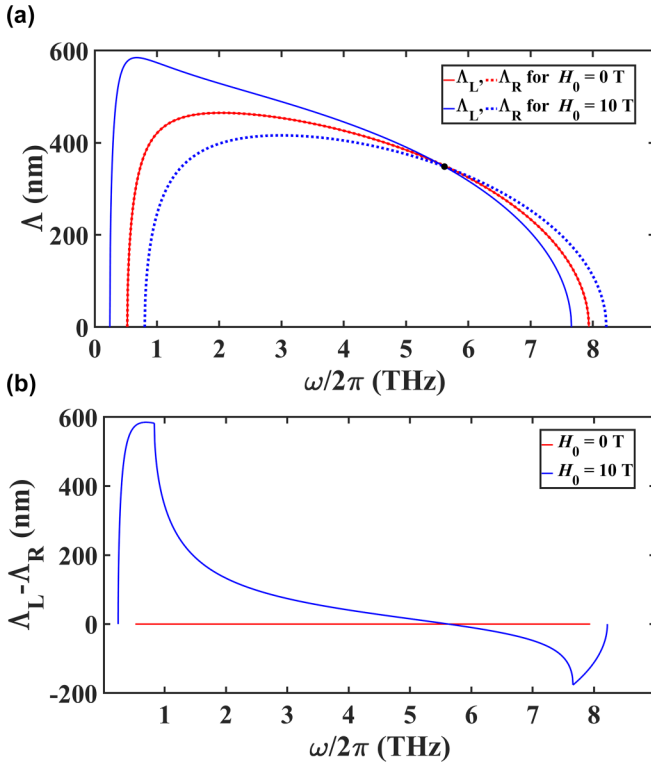
(a)

(b)

FIG. 2. (a) Frequency dependence of the attenuation lengths of the LPSW (solid lines) and RPSW (dotted lines) for the external field $H_0 = 0$ (red) and $H_0 = 10$ T (blue). (b) Frequency dependence of the attenuation length difference ($\Lambda_L - \Lambda_R$) between the LPSW and RPSW.

III. EFFECT OF THE EXTERNAL MAGNETIC FIELD

When only the external magnetic field is present, the SW dispersion relation and the attenuation length are simplified to (details are provided in the Supplemental Material [47])

$$\omega_{L/R} = \mp \gamma H_0 + \gamma \sqrt{(H_a + H_e)^2 - H_e^2 \cos^2 ak}, \quad (7)$$

$$\Lambda_{L/R} = \frac{\gamma a H_e^2 \sin(2ak)}{2(H_a + H_e)\alpha\omega_{L/R}}, \quad (8)$$

where $\omega_{L/R}$ is the frequency of the LPSW/RPSW, and $\Lambda_{L/R}$ is the corresponding attenuation length. The magnetic field lifts the degeneracy of the LPSW and RPSW and gives rise to a frequency splitting of $2\gamma H_0$. The cutoff frequencies for LPSW and RPSW become $\omega_{cL/cR} = \mp \gamma H_0 + \gamma\sqrt{H_a(H_a + 2H_e)}$. SWs with frequency below $\omega_{cL/cR}$ cannot propagate in an antiferromagnet. When the field strength H_0 is larger than the spin-flop field $H_{SF} = \sqrt{2H_aH_e - H_a^2}$ [43], the linear AFM structure is unstable. In this work, only the linear AFM structure is considered.

The magnetic field also affects the attenuation of the LPSW and RPSW. Figure 2 shows the frequency dependence of the SW attenuation lengths when $H_0 = 0$ and 10 T. In the absence of the magnetic field, the LPSW and RPSW have the same attenuation length. The attenuation length $\Lambda_{L/R}$ increases very rapidly near the cutoff frequency ($k \to 0$). After reaching the maximum value, $\Lambda_{L/R}$ first decreases gradually
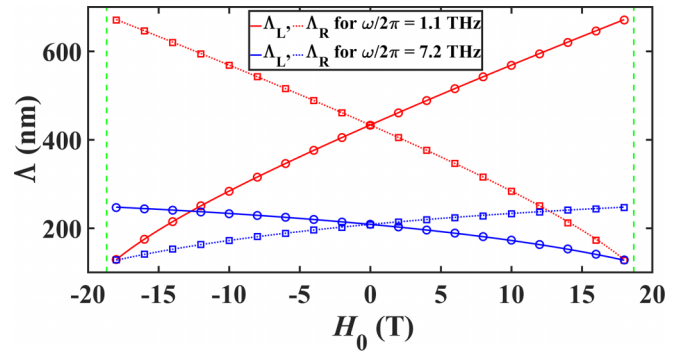

FIG. 3. Magnetic field dependence of the attenuation lengths Λ of the LPSW (solid lines) and RPSW (dotted lines) for frequencies of $\omega/2\pi = 1.1$ THz (red) and $\omega/2\pi = 7.2$ THz (blue). The circles and squares represent the results of micromagnetic simulations for LPSW and RPSW, respectively. The green vertical dashed lines indicate the value of the spin-flop field $H_{SF} \approx 18.68$ T.

and then decreases rapidly when the wave vector k approaches the boundary of the first Brillouin zone ($k \to a/2$). The fast increase/decrease of the attenuation length is related to the SW propagating velocity. Substituting the SW velocity $v_{L/R} = d\omega_{L/R}/dk$ into Eq. (8), we obtain the SW attenuation length:

$$\Lambda_{L/R} = \frac{v_{L/R}\left(1 \pm \frac{\gamma H_0}{2\omega_{L/R}}\right)}{(H_a + H_e)\gamma\alpha}. \quad (9)$$

$\Lambda_{L/R}$ is proportional to the velocity $v_{L/R}$, which increases rapidly at the center of the Brillouin zone and decreases rapidly when k approaches the boundary. When the magnetic field is applied, an additional term $(1 \pm \gamma H_0/2\omega_{L/R})$ is introduced in Eq. (9). The attenuation length of one SW mode (LPSW) is increased and the other mode (RPSW) is decreased [see Fig. 2(a)]. The attenuation length difference ($\Lambda_L - \Lambda_R$) between two SW modes is largest in the low-frequency range (near the center of the Brillouin zone), as shown in Fig. 2(b). When the frequency is between the two cutoff frequencies ω_{cL} and ω_{cR}, only one SW mode can propagate in the AFM. As the frequency increases, ($\Lambda_L - \Lambda_R$) decreases rapidly and approaches zero at a critical value $f_c = \omega_c/2\pi = 5.6$ THz, where $\Lambda_L = \Lambda_R$, and both are equal to the attenuation length without a magnetic field. After that, the increase or decrease of the SW attention lengths is reversed, i.e., the magnetic field increases the RPSW attenuation length while it decreases the LPSW one. When k approaches the boundary of the Brillouin zone, ($\Lambda_L - \Lambda_R$) approaches zero again.

The variation of the attenuation lengths Λ_L and Λ_R with the magnetic field is plotted in Fig. 3 for frequencies $\omega/2\pi = 1.1$ and 7.2 THz. It demonstrates clearly that the magnetic field enhances the attenuation of one of the SW modes and weakens that of another. Reversing the magnetic field, the situation is reversed. The results of micromagnetic simulations are also presented in Fig. 3. The details of the simulations are provided in the Supplemental Material [47]. The theoretically calculated results agree very well with the simulations.

IV. EFFECT OF THE SLONCZEWSKI-TYPE STT

The effect of Slonczewski-type STT on the SW dispersion relations is negligible in the linear approximation, and the
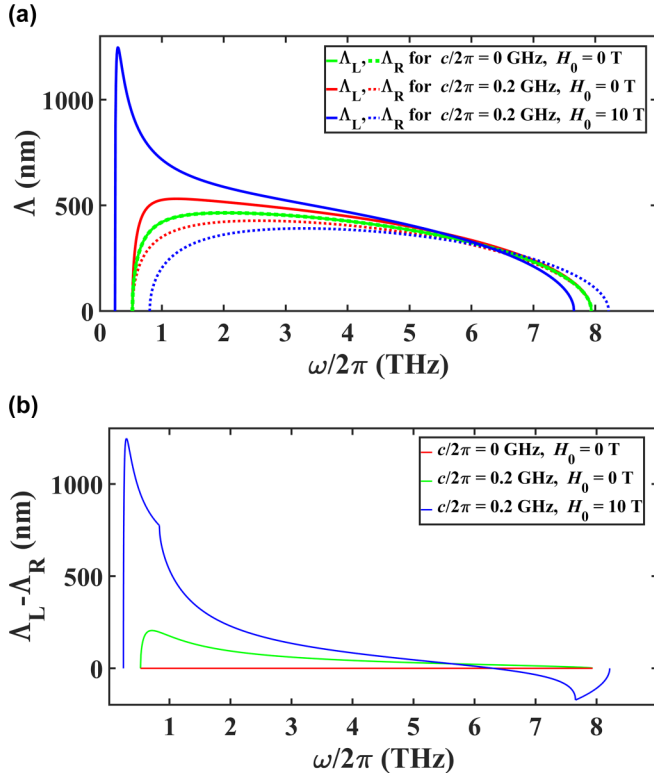
(a)

(b)

FIG. 4. (a) Frequency dependence of the attenuation lengths of the LPSW (solid lines) and RPSW (dotted lines) for $c/2\pi = 0$ and $H_0 = 0$ (red), $c/2\pi = 0.2$ GHz and $H_0 = 0$ (green), and $c/2\pi = 0.2$ GHz and $H_0 = 10$ T (blue). (b) Frequency dependence of the attenuation length difference $(\Lambda_L - \Lambda_R)$ between the LPSW and RPSW.

SW dispersion relations have the same formula as Eq. (7), meaning the Slonczewski-type STT does not lift the degeneracy of the LPSW and RPSW when $H_0 = 0$. The SW attenuation length has the following form:

$$\Lambda_{L/R} = \frac{\gamma a H_e^2 \sin(2ak)}{2(H_a + H_e)(\alpha\omega_{L/R} \mp c)}.$$
(10)

The STT increases (decreases) the attenuation length of LPSW (RPSW), and vice versa if the electric current is reversed. When $c = \pm\alpha\omega_{L/R}$, $\Lambda_{L/R}$ becomes infinite. The critical current for instability of the linear AFM structure is estimated to be [43]

$$c_- = -\alpha\gamma(H_{SF} + H_0), \quad c_+ = \alpha\gamma(H_{SF} - H_0).$$
(11)

The current strength $c = \pm\alpha\omega_{L/R}$ for infinite $\Lambda_{L/R}$ is larger than the critical current $c_\pm$ for the instability condition. So the current strength c used to manipulate the SWs is limited to $c_- < c < c_+$. In the absence of the magnetic field, the critical current is $c_+/2\pi = -c_-/2\pi = 0.52$ GHz.

Figure 4 shows the variation of the attenuation lengths Λ_L and Λ_R with the SW frequency. When $H_0 = 0$, the STT-induced variation of Λ_L and Λ_R is similar to that induced by the magnetic field. STT suppresses the attenuation of one SW mode (RPSW) and enhances that of another (LPSW). If the current is reversed, the increase or decrease in attenuation length of LPSW and RPSW is reversed as well. The largest value of $(\Lambda_L - \Lambda_R)$ is in the long-wavelength range, and it
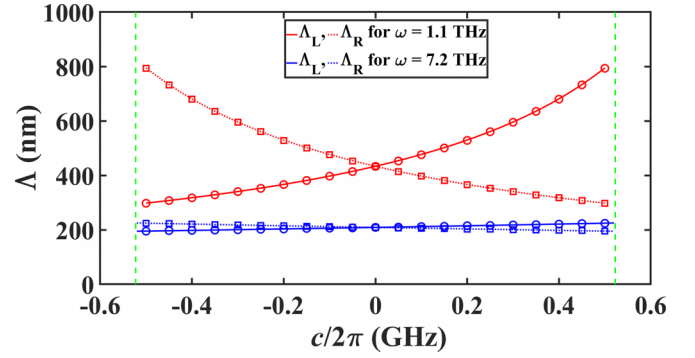

FIG. 5. Variation of the attenuation length Λ of the LPSW (solid lines) and RPSW (dotted lines) with the STT strength c for the frequencies of $\omega/2\pi = 1.1$ THz (red) and $\omega/2\pi = 7.2$ THz (blue). Circles and squares represent the results of the micromagnetic simulations for the LPSW and RPSW, respectively. The green vertical dashed lines indicate the value of the spin-flop field $H_{SF} \approx 18.68$ T.

decreases gradually with increasing frequency. If a magnetic field of $H_0 = 10$ T is applied together with the current, the degeneracy of the LPSW and RPSW is lifted, and the tuning effect of the attenuation length is enhanced significantly. A maximum $(\Lambda_L - \Lambda_R)$ up to 1 μm is reached. Of course, the tuning effect of the STT and the magnetic field can cancel each other out if the field is reversed.

The dependence of the attenuation length Λ_L and Λ_R on the STT strength c is shown in Fig. 5 for SWs with frequencies $\omega/2\pi = 1.1$ and 7.2 THz when $H_0 = 0$ and 10 T. Λ_L (Λ_R) increases (decreases) nonlinearly with c when $\omega/2\pi = 1.1$ THz, while a near linear dependence is observed for $\omega/2\pi = 7.2$ THz. When c is much smaller than $\alpha\omega_{L/R}$, the attenuation length is approximated as

$$\Lambda_{L/R} \approx \frac{\gamma a H_e^2 \sin(2ak)}{2(H_a + H_e)\alpha\omega_{L/R}}\left(1 \pm \frac{c}{\alpha\omega_{L/R}}\right).$$
(12)

Equation (12) shows a linear dependence of $\Lambda_{L/R}$ on c. The theoretical predictions agree well with the results of the micromagnetic simulations.

V. EFFECT OF THE ZHANG-LI STT

When an electric current flows in an antiferromagnet, the Zhang-Li type STT [Eq. (5)] will be introduced. The SW dispersions are derived as

$$\omega_{L/R} = \mp\gamma H_0 + \gamma\sqrt{(H_a + H_e)^2 - H_e^2\cos^2 ak} - \frac{u\sin(2ak)}{2a}.$$
(13)

The STT introduces a Doppler shift and leads to SW nonreciprocal propagation in antiferromagnets, as shown in Fig. 6(a), in which the dispersion relations of the LPSW and RPSW without a magnetic field are presented when an electric current $u = 500$ m/s is applied. But STT itself does not lift the degeneracy of the LPSW and RPSW. The degeneracy is lifted by the magnetic field H_0 as shown in Fig. 6(b).
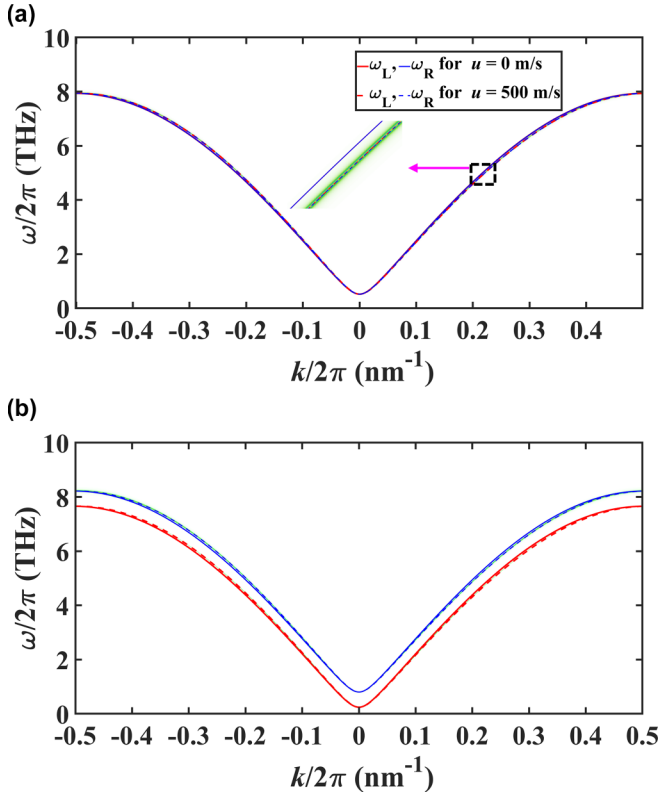
(a)

(b)

FIG. 6. Dispersion relations of the LPSW (red lines) and RPSW (blue lines) for $H_0 = 0$ (a) and $H_0 = 10$ T (b). The solid and dashed lines represent the results for the STT magnitude $u = 0$ and 500 m/s, respectively. The color-changing lines are results of micromagnetic simulations.

When only Zhang-Li type STT is present, the SW attenuation length $\Lambda_{L/R}$ can be expressed as

$$\Lambda_{L/R} = \frac{2a^2 H_e^2 \gamma^2 \sin(2ak) - 4au\omega_{L/R}\cos(2ak) - u^2\sin(4ak)}{2\gamma(H_a + H_e)[2a(\alpha\omega_{L/R}) + \beta u\sin(2ak)]}.$$

(14)

Equation (14) indicates that the Zhang-Li STT has the same effect on the LPSW and RPSW modes. Figures 7(a) and 7(d) show the calculated $\Lambda_{L/R}$ according to Eq. (13). Both the LPSW and RPSW attenuation lengths are increased (or decreased) at the same time by Zhang-Li STT, which is different from the effect of Slonczewski-type STT, where the attenuation length of one SW mode is increased while the other is decreased. Moreover, the $\Lambda_{L/R}$ is strongly dependent on the nonadiabatic STT coefficient β [see Fig. 7(d)]. $\Lambda_{L/R}$ is increased significantly when the current u approaches the critical current $u_c = \frac{-2a\alpha\omega_{L/R}}{\beta\sin(2ak)}$ of SW instability [45,50].

The LPSW and RPSW attenuation lengths cannot be manipulated separately by Zhang-Li STT. However, if a magnetic field is applied together with the Zhang-Li STT, the degeneracy of the LPSW and RPSW is lifted, and the LPSW and RPSW have different attenuation lengths, as indicated by Figs. 7(b) and 7(e). Importantly, the LPSW and RPSW have different critical current u_c for instability:

$$u_{cL} = -\frac{2a\alpha\omega_L}{\beta\sin(2ak)}, \quad u_{cR} = -\frac{2a\alpha\omega_R}{\beta\sin(2ak)}.$$

(15)

When the applied current is close to the critical current u_{cL}, the LPSW attenuation length is increased greatly, while for the RPSW mode the increase in the attenuation length is much less [see Fig. 7(e)]. A very large $(\Lambda_L - \Lambda_R)$ can be obtained. Reversing the magnetic field, the opposite manipulation for the LPSW and RPSW attenuation lengths can be achieved. A similar effect can be realized by applying the Slonczewski-type STT together with the Zhang-Li STT as shown in Figs. 7(c) and 7(f). The Slonczewski-type STT also leads to different critical currents u_{cL} and u_{cR} for the LPSW and RPSW instability, which can be expressed as

$$u_{cL} = \frac{2a(c - \alpha\omega_L)}{\beta\sin(2ak)}, \quad u_{cR} = \frac{2a(-c - \alpha\omega_R)}{\beta\sin(2ak)}.$$

(16)

As shown in Figs. 7(d)–7(f), when $\beta = 0.2$, a small current ($u < 100$ m/s) can realize the effective control of the LPSW and RPSW propagation. The strong influence of the nonadiabatic STT coefficient β on the critical currents for the SW instability, and thus on the SW attenuation length, means materials with large β are advantageous for the manipulation of the LPSW and RPSW in an antiferromagnet.

VI. SPIN FILTER

The effective manipulation of the attenuation length $\Lambda_{L/R}$ means that we can control the SW polarization in antiferromagnetism and exploit it to design novel AFM magnonic devices. Here, based on the obtained results, we propose a magnonic spin filter that can preserve one SW polarization and filter out the other. The schematics of the magnonic spin filter is shown in Fig. 8(a). A heavy-metal Pt is placed on the AFM stripe. An electric current flows in an antiferromagnet from left to right, and it provides the Zhang-Li STT. The electric current flowing in the heavy metal yields a spin current due to the spin Hall effect. When this spin current enters into the antiferromagnet, it will produce a Slonczewski-type STT (dampinglike spin-orbit torque) acting on the antiferromagnet. The sign of the Slonczewski-type STT [Eq. (4)] can be changed by reversing the direction of the current in the Pt layer. As the spin-orbit torque is an interfacial effect and the Zhang-Li STT is a body effect, it is reasonable to assume that the two spin currents are independent from each other [51,52]. The SWs are generated by an oscillating magnetic field $h(t)$ at the left end of the AFM chain. The filtered SW signals are detected at the right end.

Figure 8(b) shows the trajectory of the magnetization precession at the left end of the antiferromagnet. The large eccentricity of the ellipse means the precession is the superposition of the LPSW and RPSW. Figure 8(c) shows the precession trajectory of the magnetization 2450 nm away from the left end. Here we set the amplitude of the Zhang-Li STT as $u = -90$ m/s and $\beta = 0.2$, and the strength of the Slonczewski-type STT as $c/2\pi = 0.4$ GHz. A nearly left-handed circular trajectory is obtained, meaning the RPSW is filtered out. If the electric current in the Pt layer is reversed, the LPSW will be filtered out, and only the RPSW can reach the right output terminal, as shown in Fig. 8(d). In this way, we can obtain a pure spin-up or spin-down magnonic spin current in the antiferromagnet.
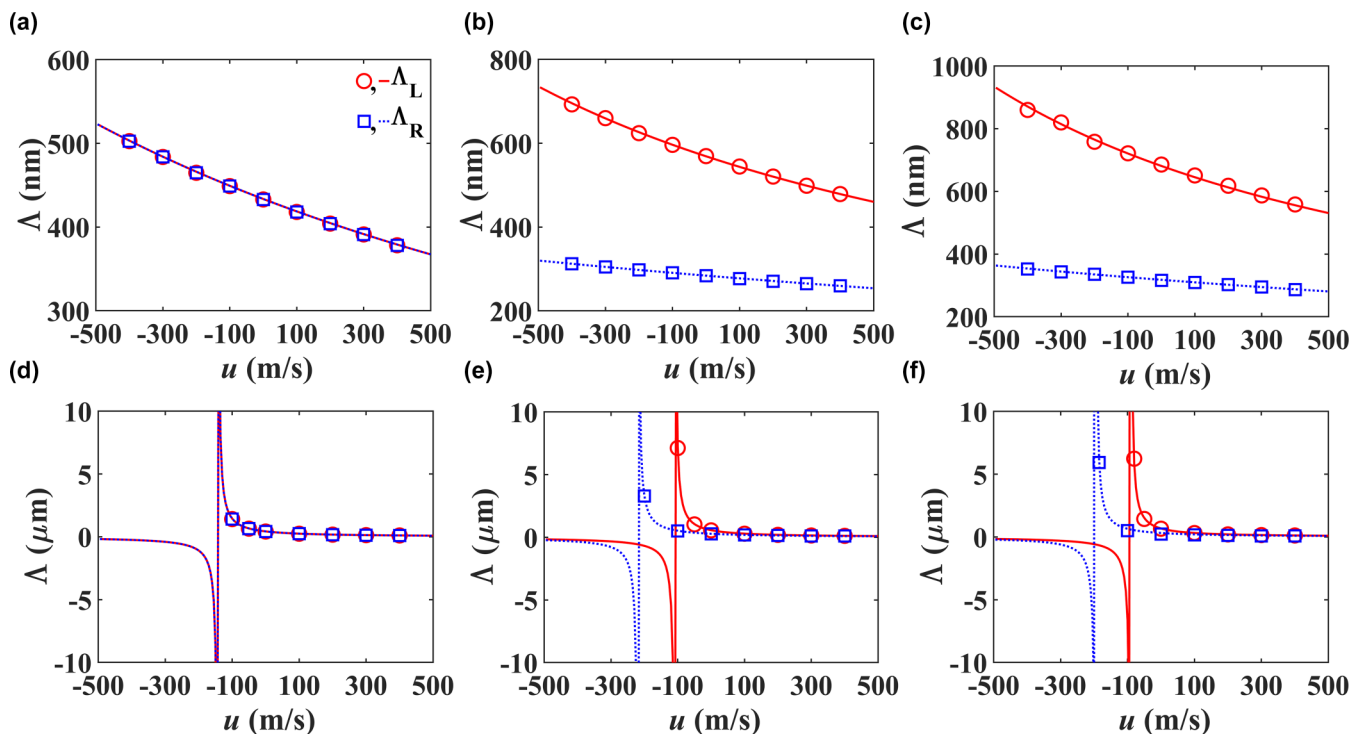
FIG. 7. Variation of the attenuation lengths of the LPSW (red lines) and RPSW (blue lines) with the magnitude u of the Zhang-Li STT. (a),(d) For $c/2\pi = 0$ and $H_0 = 0$; (b),(e) for $c/2\pi = 0$ and $H_0 = 10$ T; (c),(f) for $c/2\pi = 0.4$ GHz and $H_0 = 0$. The upper and lower rows represent the results for $\beta = 0.01$ and 0.2, respectively. Circles and squares represent the results of the micromagnetic simulations for LPSW and RPSW, respectively. The SW frequency is fixed at $\omega/2\pi = 1.1$ THz.
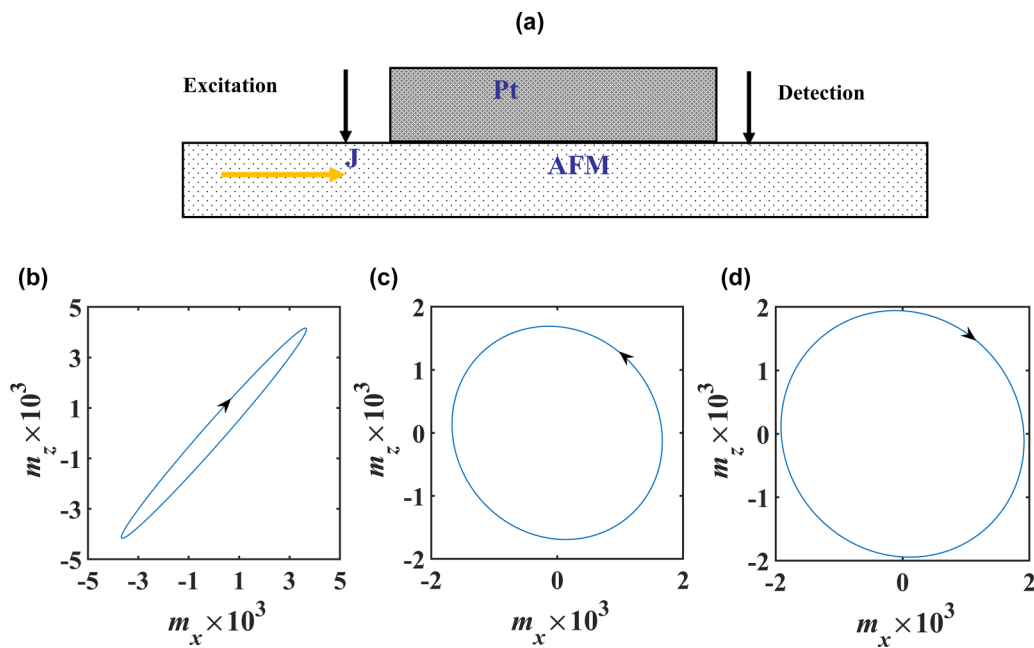

FIG. 8. (a) Schematics of the magnonic spin filter. (b)–(d) Trajectories of the magnetization precession at the position of driving field (b) and at the output terminal (c) ($c/2\pi = 0.4$ GHz, $u = -90$ m/s) and (d) ($c/2\pi = -0.4$ GHz, $u = -90$ m/s). The SW frequency is $\omega/2\pi = 1.1$ THz.

VII. CONCLUSIONS

To conclude, we study the manipulating effect of the Slonczewski-type and Zhang-Li type STTs as well as the external magnetic field on the LPSW and RPSW propagating in an antiferromagnet using analytical calculations and micromagnetic simulations. We find that the Zhang-Li STT leads to the Doppler shift of the LPSW and RPSW but does not lift their degeneracy. The attenuation of both the LPSW and RPSW can be enhanced or weakened depending on the direction of the electric current. The Slonczewski-type STT has almost no effect on the dispersion relation of LPSW and RPSW, while it can tune the attenuation of the LPSW and RPSW separately, i.e., it increases the attenuation length of one SW mode and decreases that of another mode simultaneously. Using the combined effect of the two kinds of STTs or the STT and the external magnetic field, we can control the attenuation of the LPSW and RPSW separately, thus we can manipulate the polarization of SWs and realize the generation of magnonic spin current. Based on the findings, we suggest a magnon spin filter that can filter out one of the SW modes and preserve the other one, thus generating a pure magnonic spin current in the antiferromagnet. Our studies provide important theoretical references for manipulating the SWs in antiferromagnets, and they are helpful for designing various novel AFM magnonic devices

[1] A. H. MacDonald and M. Tsoi, Antiferromagnetic metal spintronics, Philos. Trans. R. Soc. A **369**, 3098 (2011).

[2] E. V. Gomonay and V. M. Loktev, Spintronics of antiferromagnetic systems, Low Temp. Phys. **40**, 17 (2014).

[3] T. Jungwirth, X. Marti, P. Wadley, and J. Wunderlich, Antiferromagnetic spintronics, Nat. Nanotech. **11**, 231 (2016).

[4] H. Bai, X. Zhou, Y. Zhou, X. Chen, Y. You, F. Pan, and C. Song, Functional antiferromagnets for potential applications on high-density storage and high frequency, J. Appl. Phys. **128**, 210901 (2020).

[5] V. Baltz, A. Manchon, M. Tsoi, T. Moriyama, T. Ono, and Y. Tserkovnyak, Antiferromagnetic spintronics, Rev. Mod. Phys. **90**, 015005 (2018).

[6] T. Jungwirth, J. Sinova, A. Manchon, X. Marti, J. Wunderlich, and C. Felser, The multiple directions of antiferromagnetic spintronics, Nat. Phys. **14**, 200 (2018).

[7] S. M. Rezende, A. Azevedo, and R. L. Rodríguez-Suárez, Introduction to antiferromagnetic magnons, J. Appl. Phys. **126**, 151101 (2019).

[8] P. Wadley, B. Howells, J. Železný, C. Andrews, V. Hills, R. P. Campion, V. Novák, K. Olejník, F. Maccherozzi, S. S. Dhesi, S. Y. Martin, T. Wagner, J. Wunderlich, F. Freimuth, Y. Mokrousov, J. Kuneš, J. S. Chauhan, M. J. Grzybowski, A. W. Rushforth, K. W. Edmonds, B. L. Gallagher, and T. Jungwirth, Electrical switching of an antiferromagnet, Science **351**, 587 (2016).

[9] J. Železný, H. Gao, K. Výborný, J. Zemen, J. Mašek, A. Manchon, J. Wunderlich, J. Sinova, and T. Jungwirth, Relativistic Néel-order fields induced by electrical current in antiferromagnets, Phys. Rev. Lett. **113**, 157201 (2014).

[10] X. Z. Chen, R. Zarzuela, J. Zhang, C. Song, X. F. Zhou, G. Y. Shi, F. Li, H. A. Zhou, W. J. Jiang, F. Pan, and Y. Tserkovnyak, Antidamping-torque-induced switching in biaxial antiferromagnetic insulators, Phys. Rev. Lett. **120**, 207204 (2018).

[11] Y. Cheng, S. Yu, M. Zhu, J. Hwang, and F. Yang, Electrical switching of tristate antiferromagnetic Néel order in α-Fe$_2$O$_3$ epitaxial films, Phys. Rev. Lett. **124**, 027202 (2020).

[12] S. Dasgupta and O. A. Tretiakov, Tuning the Hall response of a noncollinear antiferromagnet via spin-transfer torques and oscillating magnetic fields, Phys. Rev. Res. **4**, L042029 (2022).

[13] I. Fina, X. Marti, D. Yi, J. Liu, J. H. Chu, C. Rayan-Serrao, S. Suresha, A. B. Shick, J. Železný, T. Jungwirth, J. Fontcuberta, and R. Ramesh, Anisotropic magnetoresistance in an antiferromagnetic semiconductor, Nat. Commun. **5**, 4671 (2014).

[14] D. Kriegner, K. Výborný, K. Olejník, H. Reichlová, V. Novák, X. Marti, J. Gazquez, V. Saidl, P. Němec, V. V. Volobuev, G. Springholz, V. Holý, and T. Jungwirth, Multiple-stable anisotropic magnetoresistance memory in antiferromagnetic MnTe, Nat. Commun. **7**, 11623 (2016).

[15] J. Fischer, O. Gomonay, R. Schlitz, K. Ganzhorn, N. Vlietstra, M. Althammer, H. Huebl, M. Opel, R. Gross, S. T. B. Goennenwein, and S. Geprägs, Spin Hall magnetoresistance in antiferromagnet/heavy-metal heterostructures, Phys. Rev. B **97**, 014417 (2018).

[16] S. Yu. Bodnar, L. Šmejkal, I. Turek, T. Jungwirth, O. Gomonay, J. Sinova, A. A. Sapozhnik, H.-J. Elmers, M. Kläui, and M. Jourdan, Writing and reading antiferromagnetic Mn$_2$Au by Néel spin-orbit torques and large anisotropic magnetoresistance, Nat. Commun. **9**, 348 (2018).

[17] S. M. Wu, W. Zhang, A. KC, P. Borisov, J. E. Pearson, J. S. Jiang, D. Lederman, A. Hoffmann, and A. Bhattacharya, Antiferromagnetic spin seebeck effect, Phys. Rev. Lett. **116**, 097204 (2016).

[18] S. Seki, T. Ideue, M. Kubota, Y. Kozuka, R. Takagi, M. Nakamura, Y. Kaneko, M. Kawasaki, and Y. Tokura, Thermal generation of spin current in an antiferromagnet, Phys. Rev. Lett. **115**, 266601 (2015).

[19] J. Li, H. T. Simensen, D. Reitz, Q. Sun, W. Yuan, C. Li, Y. Tserkovnyak, A. Brataas, and J. Shi, Observation of magnon polarons in a uniaxial antiferromagnetic insulator, Phys. Rev. Lett. **125**, 217201 (2020).

[20] R. Cheng, J. Xiao, Q. Niu, and A. Brataas, Spin pumping and spin-transfer torques in antiferromagnets, Phys. Rev. Lett. **113**, 057601 (2014).

[21] J. Li, C. B. Wilson, R. Cheng, M. Lohmann, M. Kavand, W. Yuan, M. Aldosary, N. Agladze, P. Wei, M. S. Sherwin, and

J. Shi, Spin current from sub-terahertz-generated antiferromagnetic magnons, Nature (London) **578**, 70 (2020).

[22] P. Vaidya, S. Morley, J. van Tol, Y. Liu, R. Cheng, A. Brataas, D. Lederman, and E. del Barco, Subterahertz spin pumping from an insulating antiferromagnet, Science **368**, 160 (2020).

[23] Z. Y. Qiu, D. Z. Hou, J. Barker, K. Yamamoto, O. Gomonay, and E. Saitoh, Spin colossal magnetoresistance in an antiferromagnetic insulator, Nat. Mater. **17**, 577 (2018).

[24] X.-G. Wang, Y.-Z. Nie, L. Chotorlishvili, Q.-L. Xia, J. Berakdar, and G.-H. Guo, Electron-magnon spin conversion and magnonic spin pumping in an antiferromagnet/heavy metal heterostructure, Phys. Rev. B **103**, 064404 (2021).

[25] Y. Wang, D. Zhu, Y. Yang, K. Lee, R. Mishra, G. Go, S.-H. Oh, D.-H. Kim, K. Cai, E. Liu, S. D. Pollard, S. Shi, J. Lee, K. L. Teo, Y. Wu, K.-J. Lee, and H. Yang, Magnetization switching by magnon-mediated spin torque through an antiferromagnetic insulator, Science **366**, 1125 (2019).

[26] X.-G. Wang, L.-L. Zeng, Y.-Z. Nie, Z. Luo, Q.-L. Xia, and G.-H. Guo, Manipulation of polarized magnon transmission in a trilayer magnonic spin valve, Phys. Rev. B **105**, 094416 (2022).

[27] J. Lan, W. Yu, and J. Xiao, Antiferromagnetic domain wall as spin wave polarizer and retarder, Nat. Commun. **8**, 178 (2017).

[28] O. V. Pylypovskyi, D. Y. Kononenko, K. V. Yershov, U. K. Rößler, A. V. Tomilo, J. Fassbender, J. van den Brink, D. Makarov, and D. D. Sheka, Curvilinear one-dimensional antiferromagnets, Nano Lett. **20**, 8157 (2020).

[29] E. Haltz, J. Sampaio, S. Krishnia, L. Berges, R. Weil, A. Mougin, and A. Thiaville, Quantitative analysis of spin wave dynamics in ferrimagnets across compensation points, Phys. Rev. B **105**, 104414 (2022).

[30] C. Jia, M. Chen, A. F. Schäffer, and J. Berakdar, Chiral logic computing with twisted antiferromagnetic magnon modes, npj Comput. Mater. **7**, 101 (2021).

[31] R. Cheng, M. W. Daniels, J.-G. Zhu, and D. Xiao, Antiferromagnetic spin wave field-effect transistor, Sci. Rep. **6**, 24223 (2016).

[32] S. M. Rezende, *Fundamentals of Magnonics* (Springer, Cham, Switzerland, 2020).

[33] X. Liang, Z. Wang, P. Yan, and Y. Zhou, Nonreciprocal spin waves in ferrimagnetic domain-wall channels, Phys. Rev. B **106**, 224413 (2022).

[34] S. Dasgupta and J. Zou, Zeeman term for the Néel vector in a two sublattice antiferromagnet, Phys. Rev. B **104**, 064415 (2021).

[35] S. K. Kim, Y. Tserkovnyak, and O. Tchernyshyov, Propulsion of a domain wall in an antiferromagnet by magnons, Phys. Rev. B **90**, 104406 (2014).

[36] J. C. Slonczewski, Current-driven excitation of magnetic multilayers, J. Magn. Magn. Mater. **159**, L1 (1996).

[37] J. C. Slonczewski, Excitation of spin waves by an electric current, J. Magn. Magn. Mater. **195**, L261 (1999).

[38] L. Berger, Emission of spin waves by a magnetic multilayer traversed by a current, Phys. Rev. B **54**, 9353 (1996).

[39] S. Zhang and Z. Li, Roles of nonequilibrium conduction electrons on the magnetization dynamics of ferromagnets, Phys. Rev. Lett. **93**, 127204 (2004).

[40] Y. Yamane, J. Ieda, and J. Sinova, Spin-transfer torques in antiferromagnetic textures: Efficiency and quantification method, Phys. Rev. B **94**, 054409 (2016).

[41] F. Keffer, H. Kaplan, and Y. Yafet, Spin waves in ferromagnetic and antiferromagnetic materials, Am. J. Phys. **21**, 250 (1953).

[42] E. G. Tveten, T. Müller, J. Linder, and A. Brataas, Intrinsic magnetization of antiferromagnetic textures, Phys. Rev. B **93**, 104408 (2016).

[43] H. V. Gomonay and V. M. Loktev, Spin transfer and current-induced switching in antiferromagnets, Phys. Rev. B **81**, 144427 (2010).

[44] M. W. Daniels, W. Guo, G. M. Stocks, D. Xiao, and J. Xiao, Spin-transfer torque induced spin waves in antiferromagnetic insulators, New J. Phys. **17**, 103039 (2015).

[45] S.-M. Seo, K.-J. Lee, H. Yang, and T. Ono, Current-induced control of spin-wave attenuation, Phys. Rev. Lett. **102**, 147202 (2009).

[46] J.-H. Moon, S.-M. Seo, K.-J. Lee, K.-W. Kim, J. Ryu, H.-W. Lee, R. D. McMichael, and M. D. Stiles, Spin-wave propagation in the presence of interfacial Dzyaloshinskii-Moriya interaction, Phys. Rev. B **88**, 184404 (2013).

[47] See Supplemental Material at http://link.aps.org/supplemental/10.1103/PhysRevB.108.134432 for an analytical derivation of the dispersion relations and attenuation lengths of the spin waves in antiferromagnets and the details of the micromagnetic simulations.

[48] J. Barker and O. A. Tretiakov, Static and dynamical properties of antiferromagnetic Skyrmions in the presence of applied current and temperature, Phys. Rev. Lett. **116**, 147203 (2016).

[49] A. Vansteenkiste, J. Leliaert, M. Dvornik, M. Helsen, F. Garcia-Sanchez, and B. V. Waeyenberge, The design and verification of MuMax3, AIP Adv. **4**, 107133 (2014).

[50] Z.-W. Zhou, X.-G. Wang, Y.-Z. Nie, Q.-L. Xia, Z.-M. Zeng, and G.-H. Guo, Left-handed polarized spin waves in ferrimagnets induced by spin-transfer torque, Phys. Rev. B **99**, 014420 (2019).

[51] R. Mondal, M. Berritta, and P. M. Oppeneer, Unified theory of magnetization dynamics with relativistic and nonrelativistic spin torques, Phys. Rev. B **98**, 214429 (2018).

[52] C. R. MacKinnon, S. Lepadatu, T. Mercer, and P. R. Bissell, Role of an additional interfacial spin-transfer torque for current-driven Skyrmion dynamics in chiral magnetic layers, Phys. Rev. B **102**, 214408 (2020).